PHILOSOPHICAL TRANSACTIONS OF THE ROYAL SOCIETY A MATHEMATICAL, PHYSICAL & ENGINEERING SCIENCES

The CNOC2 field galaxy redshift survey

R. G Carlberg, H. K. C. Yee, S. L. Morris, H. Lin, M. Sawicki, G. Wirth, D. Patton, C. W. Shepherd, E. Ellingson, D. Schade, C. J. Pritchet and F. D. A. Hartwick

Phil. Trans. R. Soc. Lond. A 1999 **357**, 167-183
doi: 10.1098/rsta.1999.0321

THE ROYAL SOCIETY

The CNOC2 field galaxy redshift survey

By R. G. Carlberg[1,5,†], H. K. C. Yee[1,†], S. L. Morris[2,†], H. Lin[1,†], M. Sawicki[1,†], G. Wirth[3,†], D. Patton[3,†], C. W. Shepherd[1], E. Ellingson[4,†], D. Schade[2,†], C. J. Pritchet[3] and F. D. A. Hartwick[3]

[1]*Department of Astronomy, University of Toronto, 60 St George Street, Toronto, Ontario, Canada M5S 1A1*

[2]*Dominion Astrophysical Observatory, 5071 W. Saanich Road, Victoria, British Columbia, Canada V8X 4M6*

[3]*Department of Physics and Astronomy, University of Victoria, PO Box 3055, Victoria, British Columbia, Canada V8W 3P6*

[4]*Center for Astrophysics and Space Astronomy CB 389, University of Colorado, Boulder, CO 80309, USA*

[5]*Observatories of the Carnegie Institution of Washington, 813 Santa Barbara Street, Pasadena, CA 91109, USA*

The second Canadian Network for Observational Cosmology (CNOC) galaxy redshift survey, CNOC2, is designed to investigate the relations between the dramatic evolution of field galaxies and their clustering over the redshift range 0–0.7. The sample of about 6000 galaxies with accurate velocities is spread over four sky patches with a total area of about 1.5 deg^2. Here we report preliminary results based on two of the sky patches and within the redshift range of 0.12–0.55. After classifying the galaxy spectral energy distributions relative to non-evolving references, we find that the early and intermediate-type populations can be described with nearly pure luminosity evolution, whereas the late-type population requires nearly pure density evolution. The spatial two-point correlation functions have a strong colour dependence with scale, and a weaker, apparently scale-free, luminosity dependence. The population most likely to be conserved with redshift is the high-luminosity galaxies. In particular, we choose galaxies with $M_{\rm R}^{k,e} \leqslant -20$ mag as our tracer population. We find that the evolution of the clustered density in proper coordinates at $r \lesssim 10\,h^{-1}$ Mpc, $\rho_{\rm gg} \propto r_0^{\gamma}(1+z)^3$, is best described as a 'declustering', proportional to $(1+z)^{0.6\pm0.4}$; or, equivalently, there is a weak growth of clustering in co-moving coordinates, $x_0 \propto (1+z)^{-0.3\pm0.2}$. This conclusion is supported by the pairwise peculiar velocities, which show no significant change with redshift. The cosmic virial theorem applied to the CNOC2 data gives $Q_3\Omega_{\rm M}/b = 0.11 \pm 0.04$, where Q_3 is the three-point correlation parameter and b the bias.

Keywords: cosmology; large-scale structure; galaxy evolution; large-scale structure, evolution of; redshift surveys; galaxy groups

† Visiting Astronomer, Canada–France–Hawaii Telescope, which is operated by the National Research Council of Canada, le Centre National de Recherche Scientifique, and the University of Hawaii.

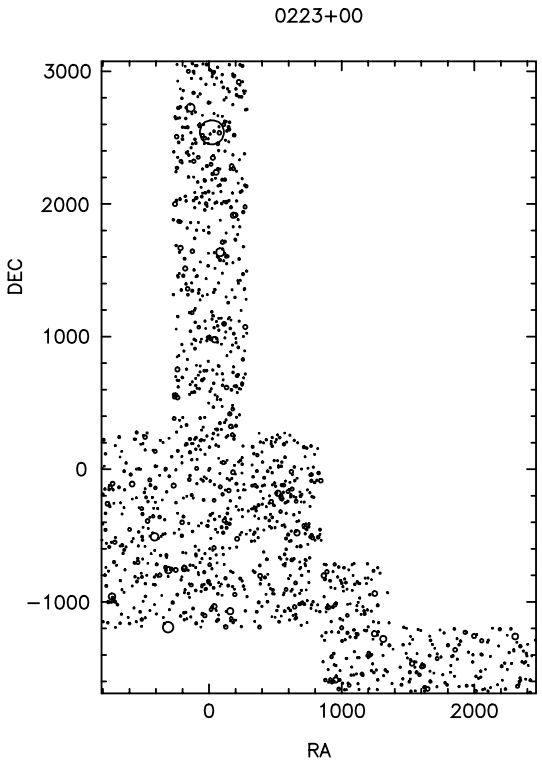

Figure 1. The distribution on the sky, in seconds of arc, of the galaxies with redshifts and $m_{\rm R} \leqslant 21.7$ mag in 19 of the 20 fields in the 0223+00 patch.

1. The motivation and design of the survey

The best test of theories of structure evolution is to observe the evolution of both galaxies and their clustering. The Canadian Network for Observational Cosmology (CNOC) field galaxy redshift survey is designed to investigate nonlinear clustering dynamics and its relation to galaxy evolution on scales smaller than *ca.* 20 h^{-1} Mpc over the $0 \leqslant z \leqslant 0.7$ range. To meet these goals requires a 'CfA-class' survey (Davis & Peebles 1983) which contains roughly 10^4 galaxies in $10^6\ h^{-3}$ Mpc^3 to allow subsampling and to provide minimal coverage of a representative set of clustering environments. For observational convenience the survey is distributed over four patches, each nominally containing 20 multi-object spectrograph (MOS) (Le Fèvre *et al.* 1994) fields of *ca.* $9' \times 8'$ on the sky. The layout (minus one field) is shown in figure 1.

The fields are observed in the UBgRI filters, with the R (Kron–Cousins) magnitudes (measured as total magnitudes (Yee 1991)) being used to define the survey. The photometric sample extends to about $m_{\rm R} = 24$ mag, with comparable depths in the other filters, except for U and I which extend to 23 mag. The spectroscopic sample is drawn from a 'mountain' version of the photometric sample with a nominal limit of $m_{\rm R} = 21.5$ mag. Each field is observed with two spectroscopic masks, the 'bright' mask extending to $m_{\rm R} \simeq 20$ mag and the 'faint' mask extending to the limiting magnitude. Slits for additional fainter objects are placed in any otherwise unoccupied areas. Together the two masks largely eliminate the problem of slit crowding and have

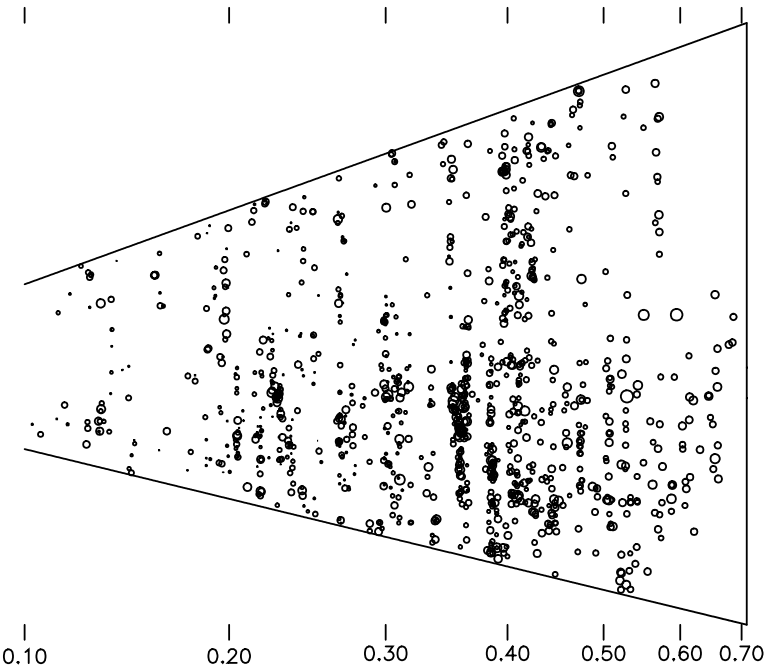

Figure 2. The line-of-sight distance versus the transverse distance in the Dec direction from the field centre, in proper coordinates, in the 0223+00 patch. 259 to 946 Dec −7.9 to 11.7 (h^{-1} proper Mpc).

the further benefit of increasing the efficiency of the observations. The spectra are band limited with a filter extending from 4400 to 6300 Å, which gives a statistically complete sample over the $0.15 \leqslant z \leqslant 0.55$ range, with emission line galaxies visible over $0 \leqslant z \leqslant 0.7$. The average completeness of the resulting redshift sample relative to the photometric sample is about 50%. The success rate for obtaining redshifts from spectra is about 85% after accounting for the fraction of objects expected to be outside our passband. The failures are mainly due to poor seeing, poor transparency and objects in the corners of the MOS. The redshift distribution for one patch is shown in figure 2.

2. Evolution of the luminosity function

The availability of UBVRI photometry (V derived from the g filter) for our sample allows us to classify CNOC2 galaxies by colour and to compute the luminosity functions (LFs) for different galaxy populations in a number of different bandpasses. Elsewhere we give details of our LF methods and descriptions of CNOC2 LF evolution results (Lin *et al*. 1999*a*) and comparison of our LF, number count and colour distribution data against a variety of galaxy evolution models (Lin *et al*. 1999*b*).

We calculate LF parameters in the $B_{\rm AB}$, R and U bands for 'early', 'intermediate' and 'late' CNOC2 galaxies, classified using fits of UBVRI colours to the galaxy spectral energy distributions (SEDs) of Coleman *et al*. (1980). The following convenient

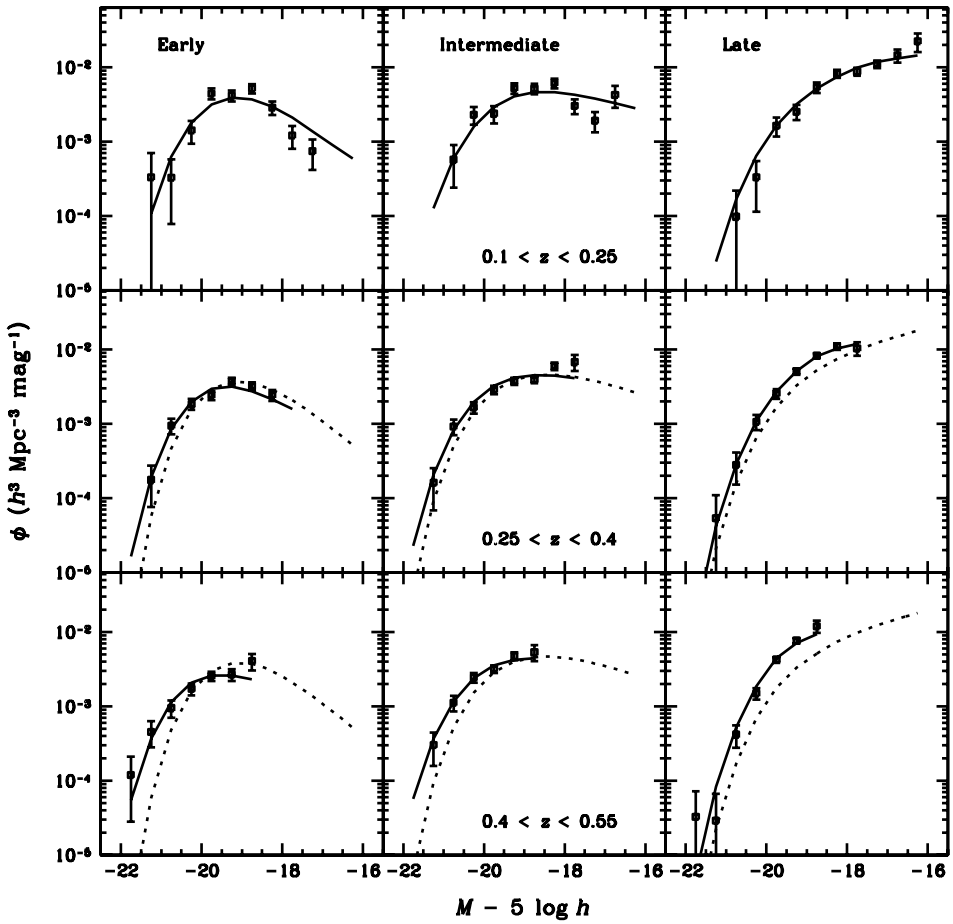

Figure 3. Evolution of the $B_{\rm AB}$ luminosity functions (solid curves and points) for early-, intermediate- and late-type CNOC2 galaxies in three redshift bins (z increases from top to bottom). Also shown are fiducial LFs (dotted curves) from the lowest redshift bin for each galaxy type. Results shown are for $q_0 = 0.1$.

model describes the LF's evolution:

$$M^*(z) = M^*(0) - Qz,$$
$$\alpha(z) = \alpha(0),$$
$$\rho(z) = \rho(0)10^{0.4Pz},$$

where M^* and α are the usual Schechter LF parameters, ρ is the galaxy number density and P and Q parametrize the rates of number density evolution and luminosity evolution, respectively. We plot our $B_{\rm AB}$ LF results in figure 3 and show 2σ P–Q error contours in figure 4. We find that the faint-end slope of the LF is steeper for late-type galaxies relative to early-type objects, consistent with previous LF studies at both intermediate and low redshifts (see, for example, Lilly *et al*. 1995; Ellis *et al*. 1996; Lin *et al*. 1996*a*). Moreover, the LFs of the early and intermediate populations evolve differently from those of late-type galaxies. Specifically, we find that the LFs of early and intermediate types show primarily positive luminosity evolution

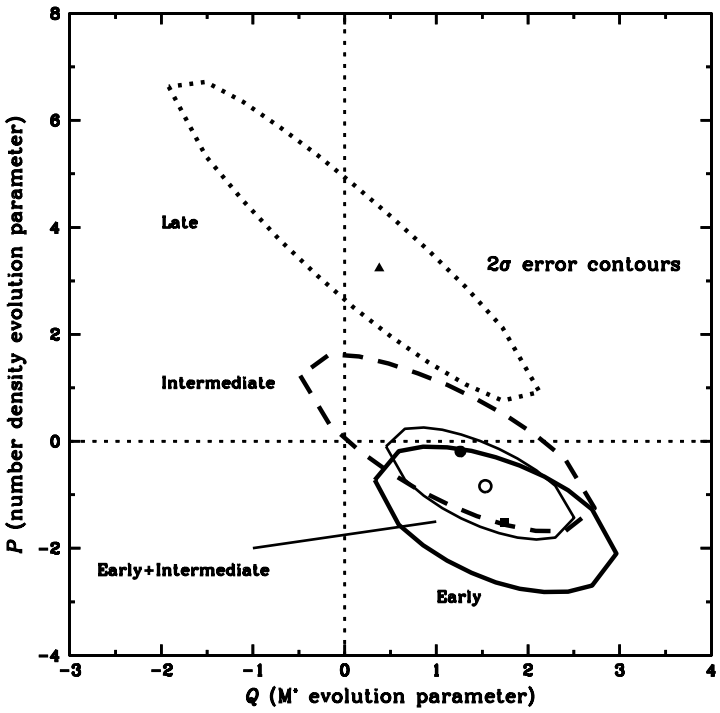

Figure 4. The two sigma confidence contours in P (number-density evolution parameter) versus Q (M^* evolution parameter) for the $B_{\rm AB}$ luminosity functions of early, intermediate, late and early + intermediate CNOC2 samples. The intersection of the horizontal and vertical dotted lines indicates no evolution; $P = Q = 0$. Results shown are for $q_0 = 0.1$; $\rho(z) = \rho(0) \times 10^{0.4Pz}$, $M^*(z) = M^*(0) - Qz$, $\alpha(z) = \alpha(0)$.

($Q \approx 1.5$) and only modest density evolution ($P \approx -1$), while the late-type LF is best fit by strong positive number-density evolution ($P \approx 3$) and little luminosity evolution ($Q \approx 0.5$). We also confirm the trend seen in previous smaller intermediate redshift samples that the luminosity density of late-type galaxies increases strongly with redshift, but that the luminosity density of early-type objects remains relatively constant with z. These general conclusions hold for either $q_0 = 0.1$ (as in the LF figures shown) or $q_0 = 0.5$.

There are various checks on the reliability of our LF results. The number counts and colour distributions for *all* $R < 21.5$ CNOC2 galaxies (not just those with redshifts in our completeness range $0.1 < z < 0.55$ used to compute the LF) are well matched once we extrapolate our LF evolution models to $z \approx 0.75$. In addition, we have verified that various systematic effects, specifically patch-to-patch variations, photometric errors, surface brightness selection, redshift incompleteness and apparent magnitude incompleteness, do not significantly affect our results.

3. Two-point correlations

The two-point correlation function, $\xi(r)$, where r is the proper coordinate separation of a galaxy pair, describes the average excess density of other galaxies around a random field galaxy (Peebles 1980). Moreover, on scales where clustering is strongly

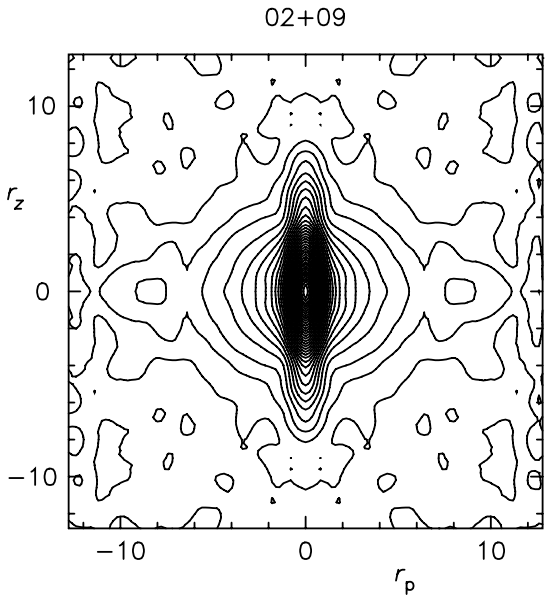

Figure 5. The two-dimensional correlation over the $0.15 \leqslant z \leqslant 0.55$ range. The plot is symmetrized about the centre and smoothed with a filter that increases with distance from the origin. The apparent flattening of the contours at large distances is not yet statistically significant.

nonlinear, the two-point correlation function is a dynamically important statistic that relates the pairwise velocity dispersion to the density parameter, $\Omega_{\rm M}$. Predictions of the relation between a nonlinear $\xi(r)$ (in the mass field) and cosmological model parameters are becoming fairly well established via n-body simulations (see, for example, Jenkins *et al.* 1997), although these are currently best viewed as model consistency tests, rather than tools for parameter estimation.

We measure the real space correlation function, $\xi(r)$, as follows. The angular separation of two galaxies, θ, at redshifts z_1 and z_2, translates into their projected separation, $r_{\rm p} = D_{\rm A}(z)\theta$, where $D_{\rm A}(z)$ is the angular size distance at redshift $z = \frac{1}{2}(z_1+z_2)$. The proper coordinate separation between the two galaxies along the line of sight, r_z, cannot be unambiguously derived from the two redshifts, since they depend on their Hubble velocities, random velocities and relative infall velocities. However, at the cost of increased noise, one can simply integrate the correlations along the line of sight to give the projected correlation function, $w_{\rm p}(r_{\rm p})$ (Davis & Peebles 1983). Specifically,

$$w_{\rm p}(r_{\rm p}) = \int_{-\infty}^{\infty} \xi(r_{\rm p}^2 + r_z^2)^{1/2}\, {\rm d}r_z.$$

For the particular case that $\xi(r) = (r_0/r)^\gamma$, then (Peebles 1980)

$$\frac{w_{\rm p}(r_{\rm p})}{r_{\rm p}} = \frac{\Gamma(\frac{1}{2})\Gamma(\frac{1}{2}(\gamma-1))}{\Gamma(\frac{1}{2}\gamma)(r_0/r_{\rm p})^{\gamma-1}}.$$

For a data-set with fairly high redshift completeness, one usually does not want to extend the r_z sum to infinity since that would decrease the overall signal to noise as distant uncorrelated pairs are added. The logic of our choice of an r_z cut-off is

roughly as follows. The cut-off must be at least large enough to include the random pairwise velocities along the line of sight, say $H(z)r_z \geqslant 3\sigma_{12}$, where

$$H(z) = H_0\sqrt{(1+z)^3\Omega_{\rm M} + (1+z)^2(1-\Omega_{\rm M})}$$

is the Hubble constant at redshift z (for $\Lambda = 0$). For a pairwise random velocity of about 300 km s^{-1} this sets a lower limit of approximately 10 h^{-1} Mpc for the r_z cut-off. If $\xi(r)$ really was a single power law to very large separations then cut-off would have to be very large. However, modelling below the line-of-sight power spectrum shows that there must be a decrease in the correlation between 30 and 100 h^{-1} Mpc. Empirically we find that a cut-off r_z of 20–50 h^{-1} Mpc gives statistically identical results. We adopt cut-offs of 30 h^{-1} Mpc for the CNOC2 data and 50 h^{-1} Mpc for the low redshift LCRS data.

Our survey is sufficiently densely sampled, with a velocity accuracy of 100 km s^{-1} or better, that we normally derive all our results from the two-dimensional correlation function, $\xi(r_{\rm p}, r_z)$, shown in figure 5, which ratios excess pairs to the smooth background at projected separation $r_{\rm p}$ and redshift separation r_z. We estimate $\xi(r_{\rm p}, r_z)$ with the classical estimator $DD/DR - 1$ (Peebles 1980), which has the advantage of simplicity and speed. The $DD \cdot RR/(DR \cdot DR) - 1$ and $(DD - 2DR + RR)/RR$ estimators lead to no significant changes of the results presented here.

(*a*) *Luminosity and colour dependence of correlations*

The autocorrelations of red and blue galaxies (for $0.15 \leqslant z \leqslant 0.55$ and $M_{\rm R}^{k,e} \leqslant -18.5$ mag) are shown in figure 6. The sample is split at $(B-R)_0 = 1.25$ (which is used as the blue–red boundary throughout this paper). The two resulting subsamples have approximately the same number of members and nearly identical mean redshifts, 0.35, but the red subsample has a mean luminosity of $M_{\rm R} = -20.5$ mag while $M_{\rm R} = -19.8$ mag for the blue subsample. The blue galaxy autocorrelation has a characteristic scale, roughly 0.3 h^{-1} Mpc, shortward of which the blue galaxy correlation falls well below that for red galaxies. A similar, but not identical, trend in the elliptical/spiral ratio is reported in the APM (Loveday *et al*. 1995) and CfA+SSRS2 survey (Marzke, personal communication). A comparison to the pairwise velocity dispersion, *ca.* 300 km s^{-1}, suggests that the 'blue break' at 0.3 h^{-1} Mpc is the radius where field galaxies statistically join a virialized region, inside of which star formation is suppressed. The dynamics of virialization in a hierarchical cosmology is to tidally remove the outer dark matter and any imbedded baryons which are likely important in the maintenance of ongoing star formation.

The issue of luminosity dependence of correlations is an important test of theories of primordial bias associated with density 'peaks'. The observational situation is unclear at the moment. The APM survey finds about a factor of three increase in correlation for about a 2 mag change in luminosity (Loveday *et al*. 1995). We find that the LCRS (Schectman *et al*. 1996) has no significant luminosity dependence of clustering after allowance for redshift differences, over a similar range of luminosities, although it should be noted that the narrow apparent magnitude range of the LCRS is not well suited to this measurement. A mild enhancement, 35% in clustering amplitude, of the clustering of high over low luminosity galaxies is seen in the Perseus–Pisces catalogue (Giovanelli & Haynes 1991; Guzzo *et al*. 1997).

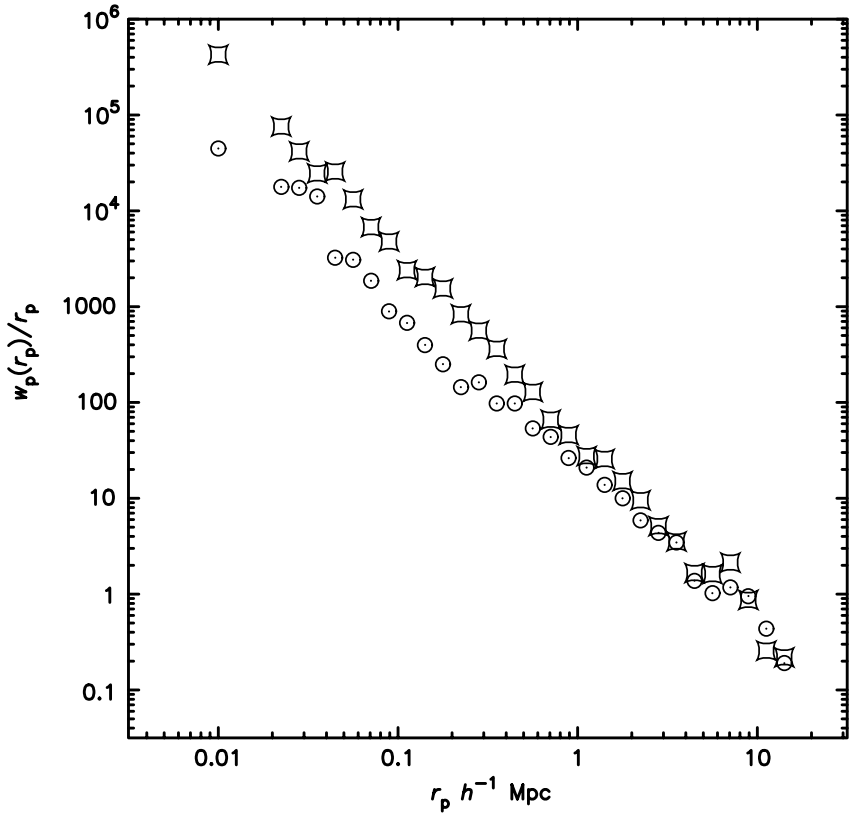

Figure 6. Autocorrelations as a function of colour. The pincushions are for red galaxies, the circles are for the blue galaxies. The blue-galaxy correlation appears to have a break at about $0.3\,h^{-1}$ Mpc.

The dependence of clustering on luminosity at $z \simeq 0.4$ is shown in figure 7. The sample is divided at $M_{\rm R} = -20$, k-corrected and evolution-corrected at an approximate rate of $M_{\rm R}(0) = M_{\rm R} - Qz$, with $Q = 1$. The mean-corrected luminosities of the two CNOC2 subsamples are -19.35 and -20.75 mag. The M_* of a Schechter fit to the luminosity function is -20.3 mag. The mean redshifts of the two samples are 0.37 and 0.34. The fitted correlation lengths are 3.7 and $2.65\,h^{-1}$ Mpc, both with $\gamma = 1.7$, or a ratio of clustering amplitudes of high to low luminosity of 1.67. These correlations are significantly larger than those estimated from the small sky area, somewhat lower luminosity, samples available previously (Le Fèvre *et al*. 1996; Shepherd *et al*. 1996; Carlberg *et al*. 1997*b*).

Within the CNOC2 data the change of correlation amplitude with luminosity is comparable in size with what is expected on the basis of galaxies of increasing luminosities being correlated with dark matter halos of increasing mass. That is, *ca.* $\xi \propto \Delta(M)^{-2} \propto M^{(n+3)/6}$, where $\Delta(M)$ is the mass field variance for spheres containing mass M, which for a perturbation spectrum, $P(k) \propto k^n$, is $\Delta \propto M^{-(n+3)/6}$. For cold-dark-matter-like (CDM-like) spectra $n \simeq -2$ on galaxy scales. We therefore expect a correlation amplitude ratio of 1.58 for the factor of four difference in luminosity of our two subsamples. That is, we attribute the observed luminosity

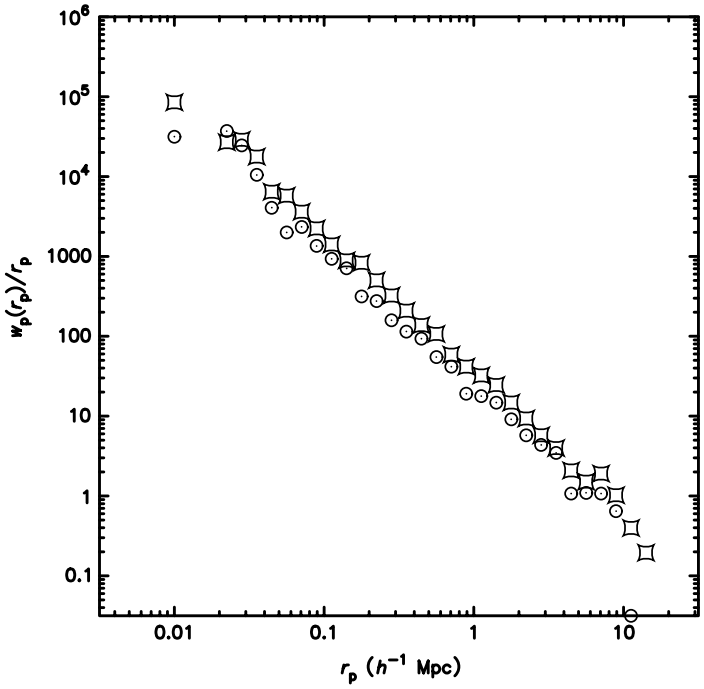

Figure 7. Autocorrelations as a function of luminosity. The pincushions are for $M_{\mathrm{R}}^{k,e} \leqslant -20$ galaxies and the circles for those between -18.5 and -20 mag.

dependence of the correlations, a factor of 1.67, as consistent with that expected from primordial 'peak heights' (Bardeen *et al*. 1986).

4. Evolution of the two-point correlation function

For the available data the evolution of galaxy correlations can be adequately described with the model $\xi(r,z) = (r_{00}/r)^{\gamma}(1+z)^{-(3+\epsilon)}$, where the lengths are measured in proper units. This double power-law model does not allow any variation of the correlation slope, γ, with redshift. The model might seem theoretically naive, but it is usually a better description of the data than any available nonlinear realization of either the mass or halo clustering within a range of CDM models (Colin *et al*. 1997; Jenkins *et al*. 1997). The evolution of clustering is entirely dependent on the mass field through Ω_{M} and the relation of galaxies to the mass field. The two extreme possibilities are that galaxies are distributed like the mass (unbiased), or that galaxies are distributed like some part of virialized dark matter halos, in which case they are biased. There are then three very general possibilities for the evolution of clustering: (i) $\epsilon \simeq 0$ for unbiased clustering if Ω_{M} is low; (ii) $\epsilon \simeq 1$ for unbiased clustering if $\Omega_{\mathrm{M}} \simeq 1$; and (iii) $\epsilon \simeq -1$ for dark matter halo clustering, with weak Ω_{M} dependence. The case of $\epsilon = 0$ separates the regime of clustering build-up to the present, $\epsilon > 0$, from an apparent clustering decrease, $\epsilon < 0$ (likely a result of merging). N-body simulations verify this general picture, although there remains considerable uncertainty as to how galaxies are related to the dark matter distribution.

A primary issue in studying the evolution of correlations is to be able to identify the same population at different redshifts, since both luminosity and colour dependence

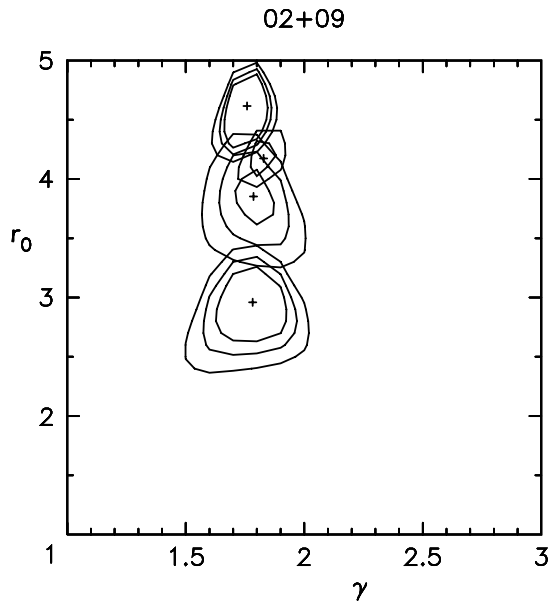

Figure 8. The fitted r_0 and γ for high-luminosity galaxies from the LCRS and CNOC2 samples. The mean redshift, from top to bottom is 0.080, 0.135, 0.28, and 0.43. Contours are 68, 90 and 99% confidence levels.

of clustering can mimic or mask the desired effect. An empirical definition of a galaxy population that is statistically fairly well conserved over our redshift range is the high luminosity galaxies, $M_{\rm R}^{k,e} \leqslant -20$. The LFs indicate that these are far better than lower luminosity galaxies to being a certifiable mass invariant population. However, the bluest members of the high-luminosity population probably vary in mass and numbers over our redshift range. This luminosity cut has the considerable advantage that an identically defined sample can be found in the LCRS (for which colours are not presently available). Introducing this luminosity cut also allows the sample to be volume limited, which decreases the complications of the redshift dependence of selection functions.

Two-point correlation parameters, r_0 and ϵ, for a power-law correlation function of the high-luminosity galaxies are shown for various redshifts in figure 8. This redshift sequence is fit to the correlation evolution model, $r_0(z)^\gamma = r_{00}^\gamma (1+z)^{-(3+\epsilon)}$, to estimate ϵ and r_{00}, giving the result shown in figure 9. We find that $r_{00} = 5.15 \pm 0.15\, h^{-1}$ Mpc and $\epsilon = -0.6 \pm 0.4$. Our result can be restated in terms of the evolution of the correlation length in co-moving coordinates, $x_0 = r_{00}(1+z)^{-(3+\epsilon-\gamma)/\gamma)}$ as $x_0 \propto (1+z)^{-0.3\pm0.2}$. That is, a weak growth of clustering in co-moving coordinates.

These data strongly exclude clustering evolution that declines as rapidly as $\epsilon = 1$. One could erroneously infer such a rapid decline if one used a sample in which galaxies at higher redshifts are intrinsically less luminous or are on average bluer than those nearby, as is the case for the general population as a function of redshift. The rate of correlation evolution falls between the values expected for an unbiased low $\Omega_{\rm M}$ and dark-matter halos for a range of $\Omega_{\rm M}$.

It should be borne in mind that our estimate of correlation evolution is a preliminary result and that the errors will be reduced when the full sample is available.

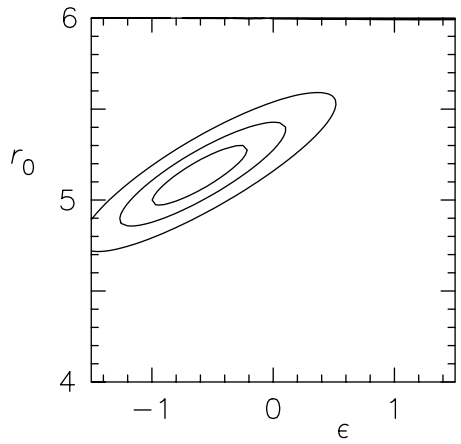

Figure 9. The fitted r_{00} at $z = 0$ and ϵ for high-luminosity galaxies from the LCRS and CNOC2 samples. The contours are 68, 90 and 99% confidence levels.

An important consideration is that the luminosity cut that defines our sample mixes together galaxies of a fairly wide range of masses and anticorrelated star-formation rates. It seems likely that low and high star-formation rate galaxies have different correlation histories. Our luminosity cut will mix some of the more rapidly evolving bluer galaxies into our sample. This possibility will be examined carefully in the full sample.

5. Galaxy pairwise velocities and their evolution

The redshift space distortions in $\xi(r_\mathrm{p}, r_z)$ reflect the dynamics of clustering. The random velocities elongate contours of $\xi(r_\mathrm{p}, r_z)$ in the line-of-sight direction, r_z, for $r_\mathrm{p} \lesssim r_0$. Infall velocities squash the contours in r_z for $r_\mathrm{p} \gtrsim r_0$. These distortions depend on Ω, and the biasing of galaxies with respect to the mass field. The data here have a local velocity accuracy of better than 100 km s^{-1}, as explicitly demonstrated using redundant spectra taken through different spectrograph slit masks. This is comparable to the velocity accuracy of surveys at low redshift. The CNOC2 survey is designed to concentrate on scales less than $10\,h^{-1}$ Mpc, so it will not provide strong limits on the infall velocities.

The pairwise peculiar velocities are derived from a model for $\xi(r_\mathrm{p}, r_z)$ following the procedures of Croft *et al.* (1999). The r_0 and γ are derived from the velocity-independent $w_\mathrm{p}(r_\mathrm{p})$. We set $\Omega_\mathrm{M} = 0.2$ in our pairwise velocity model and compute the statistical χ^2 as a function of σ_{12}. In figure 10 we show the reduced χ^2 (more than 100 degrees of freedom) versus the pairwise peculiar velocities for the LCRS sample at a mean redshift of 0.10 and the CNOC2 sample at a mean redshift of 0.36. The minimum of χ^2 rises slightly with redshift, although it is consistent with no change with redshift. The ϵ model for clustering inserted into the cosmic virial theorem (CVT, see below) predicts that $\sigma_{12}(z) \propto (1+z)^{-\epsilon/2}$, provided that the bias is not changing with redshift. We conclude that the peculiar velocities evolve in accord with that predicted from the correlation function alone. This is strong evidence that biasing of galaxies with respect to dark matter is not a large effect at these redshifts.

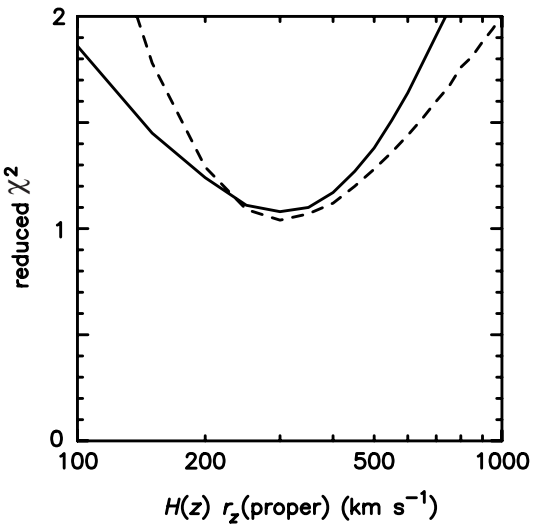

Figure 10. The χ^2 versus model pairwise peculiar velocity, σ_{12}, within the LCRS sample (solid line) at a mean redshift 0.10 and the CNOC2 sample (dashed line) at a mean redshift of 0.36.

The peculiar velocities also indicate a population dependence, as shown in figure 11. The red galaxies have a pairwise dispersion of about 350 km s^{-1}, whereas the blue galaxies have a measured dispersion of about 200 km s^{-1}. Removing the velocity errors in quadrature would reduce the pairwise velocities of blue galaxies to about 150 km s^{-1}, which is a remarkably cold population. One can speculate that in as much as accretion is necessary to promote ongoing star formation, then star formation should be suppressed in regions of strong tidal fields (virialized groups and clusters) and promoted in moderately dense regions of low-velocity dispersion.

The CVT estimates the value of $\Omega_{\rm M}$ in the field (Davis & Peebles 1983) and is an important complement to studies of clusters as $\Omega_{\rm M}$ indicators. For a power law $\xi(r)$, the CVT is (Davis & Peebles 1983; Fisher *et al*. 1994)

$$Q_3\frac{\Omega_{\rm M}}{b}=\frac{\sigma_{12}^2}{(1+z)^3r_0^\gamma r^{2-\gamma}H_0^2}\frac{4(\gamma-1)(2-\gamma)(4-\gamma)}{3J(\gamma)},$$

where Q_3 is the three-point correlation parameter, b is the linear bias of galaxy clustering relative to mass clustering, and $J(\gamma)$ is 4.14 for $\gamma=1.7$ (Peebles 1980). For $\sigma_{12}=350\pm50$ km s^{-1}, $r_0=3.2\pm0.2\,h^{-1}$ Mpc (the mean values over the $0.15\leqslant z\leqslant0.55$ range), we find $Q\Omega_{\rm M}/b=0.11\pm0.04$. For $Q=0.7$ (Davis & Peebles 1983; Bean *et al*. 1983) this indicates $\Omega_{\rm M}/b\simeq0.15\pm0.06$. This is in good accord with the results from clusters (Carlberg *et al*. 1996, 1997*a*). Because our sample finds both a uniform luminosity dependence of clustering and a scale-dependent colour effect, all galaxies cannot have $b=1$. However, it is clear that on $10\,h^{-1}$ Mpc scales and smaller, values of $b>2$ or $b<\frac{1}{2}$ are very unlikely. Moreover, this is further evidence that the matter density of the universe is $\Omega_{\rm M}\simeq0.2$ and possibly somewhat lower.

6. Ultra-large-scale power

The power spectrum of galaxy clustering on scales of 100–500 h^{-1} Mpc, is roughly the scale of the 'first Doppler peak' in the CMB fluctuation spectrum. Aside from the

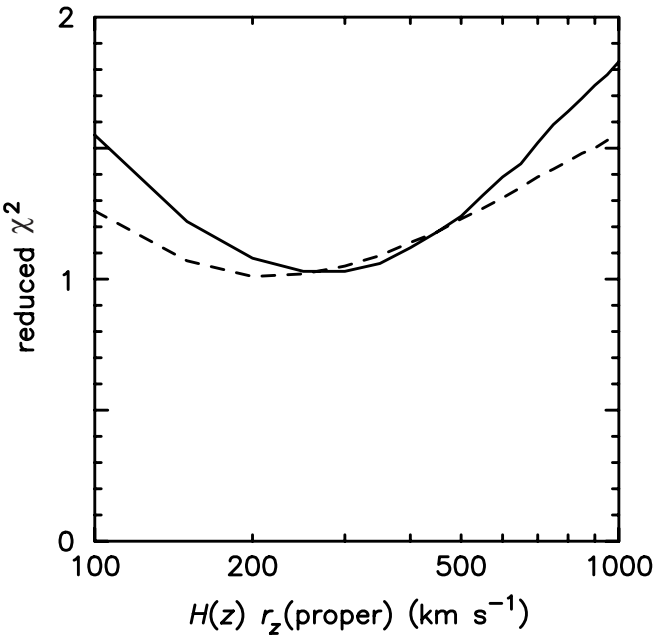

Figure 11. The χ^2 versus model pairwise peculiar velocity, σ_{12}, for the red (solid line) and blue galaxies (dashed line) within the CNOC2 sample. There is between 70 and 100 km s^{-1} added in quadrature with the true velocities.

fundamental value of knowing the power spectrum, there is a possibility that there is a feature in the spectrum on this scale. Measurement of the power spectrum on this ultra-large scale requires a survey that covers an appreciable fraction of the horizon scale. Pencil-beam surveys do just that, but only in one dimension, which leads to the problem of aliasing in of shorter scale power into the derived one-dimensional power spectrum, $P_1(k)$. In view of previous results (Broadhurst *et al.* 1990) and the fundamental interest in this statistic, we measure the one-dimensional power spectrum from the CNOC2 data and compare it to various simple models.

The one-dimensional power spectrum,

$$P_1(k) = \left| N^{-1} \sum_{i=1}^{N} \exp\left[\mathrm{i}kx_i\right] \right|^2$$

(unweighted), is shown as the upper irregular line in figure 12. At very large k_z, where the galaxies are totally uncorrelated because of velocity error, this sum tends to $1/N$ where $N \simeq 1500$ in each of our patches. The observed one-dimensional spectrum requires some care in interpretation since the one-dimensional power at a large wavenumber is an integral over the entire three-dimensional spectrum (Kaiser & Peacock 1991) whose analysis we follow here. The one-dimensional power spectrum of the smooth $n(z)$ for 10^4 randomly placed galaxies is the $W(k_z)$ window function and is shown as the lower irregular line. The power at $k_z < 0.01\,h^{-1}$ Mpc^{-1} is completely dominated by the smooth distribution of the data. At shorter wavelengths, $\lambda < 600\,h^{-1}$ Mpc, the observed power spectrum is a result of real structure.

The null hypothesis is that the one-dimensional power spectrum is simply the power spectrum of the real space correlation function, $(r_0/r)^\gamma$, as projected into

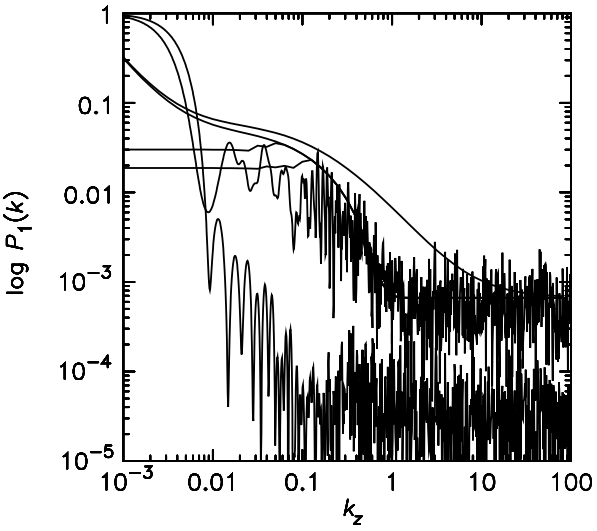

Figure 12. The one-dimensional power spectrum and related quantities. The lower irregular line is the power spectrum of the smooth $n(z)$ distribution. The upper irregular line is the power spectrum of the observed redshifts averaged over the two fields. The upper smooth line is for $(r_0/r)^{1.7}$, with $r_0 = 4.2\,h^{-1}$ Mpc (co-moving) which is modified with a Gaussian peculiar velocity distribution of 300 km s^{-1} and then the power correlation truncated at 50 and 100 h^{-1} Mpc.

these observations. The three-dimensional power spectrum is

$$P(k) = 4\pi k^{-3}(kr_0)^{\gamma}\Gamma(2-\gamma)\sin[\tfrac{1}{2}(2-\gamma)\pi].$$

To derive the window function on the sky we do a Monte Carlo evaluation of $W(k_x, k_y)$ by randomly populating the sky patches and transforming. To evaluate the predicted one-dimensional spectrum we approximate the z window function as $2\pi/L_z$, and integrate the product of the sky window function with $P(k)$. The results are displayed in figure 12, where we have added a constant shot noise of $1/N$. The unaltered spectrum does a very poor job of describing the observed spectrum. The two necessary modelling modifications are to add a random peculiar velocity and a long wavelength decline in power. The random velocities are modelled using a Gaussian (clearly not a very good description of these data) at 300 km s^{-1}. Any of the conventional CDM-type spectra roll over in the 30–100 h^{-1} Mpc range. We simply truncate the input power spectrum at 50 and 100 h^{-1} Mpc to produce the plots displayed. We can conclude that the universe is not a fractal with a fixed clustering dimension to all scales, and is otherwise consistent (at the current statistical level) with the known large-scale clustering power spectrum (Lin *et al*. 1996*b*).

7. Preliminary conclusions

The CNOC2 sample spans a range of redshifts which has dramatic galaxy evolution but in which detailed studies are readily performed. Our preliminary conclusions are discussed below.

Galaxy evolution is confirmed to be strongly differential with the blue low-mass galaxies changing significantly in their visible numbers. We find LFs similar in their overall features to previous studies (Lilly *et al*. 1995; Ellis *et al*. 1996). The new result

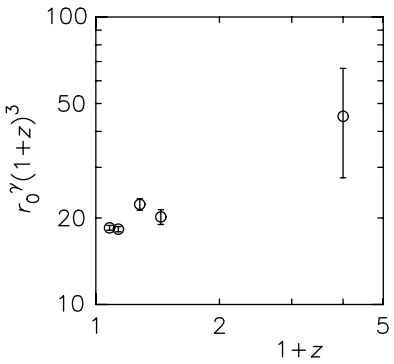

Figure 13. The evolution of the proper density of galaxies around galaxies, with the $M_{\mathrm{R}}^{k,e}$ LCRS and CNOC2 sample at low redshift and the Giavalisco *et al.* (1998) inversion at high redshift.

is that we can distinguish the character of the evolution as a function of SED types established with respect to non-evolving references. We find that the evolution of the early and intermediate SED types is well described as a pure luminosity evolution. In contrast, the late-type SED population is described as nearly pure-density evolution. It should be noted that the density evolution could be at least partly in the form of varying duty cycle of star formation.

There are two population dependences of the correlation functions. The correlation of galaxies above $M_* + 0.3$ mag is about 60% higher than those below, with a mean sample luminosity difference of a factor of four. This difference is consistent with the expected intrinsic correlation variation with mass scale in a 'peak' model for galaxies. Blue galaxies are about 50% less correlated than red galaxies on scales beyond about $0.3\,h^{-1}$ Mpc. On shorter scales blue galaxies have a break in their correlation function and become about a factor of three less correlated than red galaxies. On large scales the difference is about what one would expect from the smaller average masses of the blue galaxies. Because the $\xi(r)$ break occurs at about the average virialization scale, it suggests that the blue–red difference is an active environmental effect.

A primary result is that we find that the correlation evolution of galaxies brighter than $M_{\mathrm{R}} = -20$, where $M_* = -20.3$ mag, is well described by

$$\xi(r) = (r_{00}/r)^{\gamma}(1+z)^{-3-\epsilon},$$

where $r_{00} = 5.15 \pm 0.15\,h^{-1}$ Mpc (proper coordinates), $\gamma = 1.77 \pm 0.05$ and $\epsilon = -0.6 \pm 0.4$. That is, the physical density of galaxies around galaxies is declining slightly with redshift. Figure 13 shows that the extrapolation of our rate of clustering evolution passes smoothly through the inversion of the angular correlation of the high luminosity $z \simeq 3$ 'Steidel objects' (Giavalisco *et al.* (1998), but note Adelberger *et al.* (1998)). We note that the association of our population of objects with theirs is not secure.

The measured ϵ is completely incompatible with the $\epsilon \simeq 1$ expected for the mass field in an $\Omega_{\mathrm{M}} = 1$ universe. The result is about half-way between mass clustering in a low-density universe and the clustering evolution of the relatively high-density cores of dark matter halos (Colin *et al.* 1997). In general, an $\epsilon < 0$ implies that bias is changing with redshift, although in a low-Ω_{M} model this is a very slow function of redshift. An interpretation of the slow drop in proper density, within the context of n-body simulations, is that it is due to merging of galaxies in high-density regions.

The pairwise velocity dispersions of the luminous galaxies do not detectably evolve between $z = 0.05$ and $z = 0.4$, remaining constant at about $350\,\mathrm{km\,s^{-1}}$ (for our chosen estimator). The CVT gives $Q_3\Omega_\mathrm{M}/b = 0.11 \pm 0.04$, where Q is the three-point correlation parameter. The three-point parameter will be estimated internally from these data.

The one-dimensional power spectrum of our pencil beams requires that the observed power-law correlation at scales of less than $10\,h^{-1}$ Mpc must have a turnover at about $100\,h^{-1}$ Mpc, which is of course expected in CDM-like theories and indicated by observations of large-scale clustering at low redshift.

We set out to test theories of galaxy and structure evolution by measuring the evolution. In spite of the dramatic changes in the numbers of lower-luminosity blue galaxies, the systems of higher luminosity that dominate the stellar mass of the universe appear to be nearly a static population, having only a small change in the density of similar galaxies around them and little star formation over our redshift range.

These preliminary analyses are based on half of the eventual data for which we complete observations in May 1998. The results are likely to change somewhat (especially as other estimators are implemented and systematic errors detected and eliminated). Perhaps the primary conclusion to be drawn is that the CNOC2 data-set will be a rich sample for the study of cosmology, large-scale structure and galaxy evolution.

References

Adelberger, K., Steidel, C., Giavalisco, M., Dickinson, M., Pettini, M. & Kellogg, M. 1998 *Astrophys. J. Lett.* **505**, 18.

Bardeen, J. M., Bond, J. R., Kaiser, N. & Szalay, A. S. 1986 *Astrophys. J.* **304**, 15.

Bean, A. J., Ellis, R. S., Shanks, T., Efstathiou, G. & Peterson, B. A. 1983 *Mon. Not. R. Astr. Soc.* **205**, 605.

Broadhurst, T. J., Ellis, R. S., Koo, D. C. & Szalay, A. S. 1990 *Nature* **343**, 726.

Carlberg, R. G., Yee, H. K. C., Ellingson, E., Abraham, R., Gravel, P., Morris, S. M. & Pritchet, C. J. 1996 *Astrophys. J.* **462**, 32.

Carlberg, R. G., Yee, H. K. C. & Ellingson, E. 1997*a* *Astrophys. J.* **478**, 462.

Carlberg, R. G., Cowie, L. L., Songaila, A. & Hu, E. M. 1997*b* *Astrophys. J.* **483**, 538.

Coleman, G. D., Wu, C.-C. & Weedman, D. W. 1980 *Astrophys. J. Supp.* **43**, 393.

Colin, P., Carlberg, R. G. & Couchman, H. M. P. 1997 *Astrophys. J.* **390**, 1.

Croft, R. A. C., Dalton, G. B. & Efstathiou, G. 1999 *Mon. Not. R. Astr. Soc.* (Submitted.)

Davis, M. & Peebles, P. J. E. 1983 *Astrophys. J.* **267**, 465.

Ellis, R. S., Colless, M., Broadhurst, T., Heyl, J. & Glazebrook, K. 1996 *Mon. Not. R. Astr. Soc.* **280**, 235.

Fisher, K. B., Davis, M., Strauss, M. A., Yahil, A. & Huchra, J. P. 1994 *Mon. Not. R. Astr. Soc.* **267**, 927.

Giavalisco, M., Steidel, C. C., Adelberger, K. L., Dickinson, M. E., Pettini, M. & Kellogg, M. 1998 *Astrophys. J.* **503**, 543.

Giovanelli, R. & Haynes, M. P 1991 *A. Rev. Astr. Astrophys.* **29**, 499.

Guzzo, L., Strauss, M. A., Fisher, K. B., Giovanelli, R. & Haynes, M. P. 1997 *Astrophys. J.* **489**, 37.

Jenkins, A., Frenk, C. S., Pearce, F. R., Thomas, P. A., Colberg, J. M., White, S. D. M., Couchman, H. M. P., Peacock, J. A., Efstathiou, G. & Nelson, A. H. 1997 Preprint, astro-ph/9709010.

Kaiser, N. & Peacock, J. 1991 *Astrophys. J.* **379**, 482.

Le Fèvre, O., Crampton, D., Felenbok, P. & Monnet, G. 1994 *Astron. Astrophys.* **282**, 340.

Le Fèvre, O, Hudon, D., Lilly, S. J., Crampton, D., Hammer, F. & Tresse, L. 1996 *Astrophys. J.* **461**, 534.

Lilly, S. J., Tresse, L., Hammer, F., Crampton, D. & Le Fèvre, O. 1995 *Astrophys. J.* **455**, 108.

Lin, H., Kirshner, R. P., Schectman, S. A., Landy, S. D., Oemler, A., Tucker, D. L. & Schechter, P. L. 1996*a* *Astrophys. J.* **464**, 60.

Lin, H., Kirshner, R. P., Schectman, S. A., Landy, S. D., Oemler, A., Tucker, D. L. & Schechter, P. L. 1996*b* *Astrophys. J.* **471**, 617.

Lin, H., Yee, H. K. C., Carlberg, R. G., Morris, S. L., Sawicki, M., Patton, D., Wirth, G. & Shepherd, C. W. 1999*a* *Astrophys. J.* (Submitted.)

Lin, H., Yee, H. K. C., Carlberg, R. G., Morris, S. L., Sawicki, M., Patton, D., Wirth, G. & Shepherd, C. W. 1999*b* *Astrophys. J.* (Submitted.)

Loveday, J., Maddox, S. J., Efstathiou, G. & Peterson, B. A. 1995 *Astrophys. J.* **442**, 457.

Peebles, P. J. E. 1980 *Large scale structure of the universe*. Princeton University Press.

Shepherd, C. W., Carlberg, R. G., Yee, H. K. C. & Ellingson, E. 1996 *Astrophys. J.* **479**, 82.

Schectman, S. A., Landy, S. D., Oemler, A., Tucker, D. L., Lin, H., Kirshner, R. P. & Schechter, P. L. 1996 *Astrophys. J.* **470**, 172.

Yee, H. K. C. 1991 *Publ. Astr. Soc. Pac.* **103**, 396.

PHILOSOPHICAL TRANSACTIONS OF THE ROYAL SOCIETY A MATHEMATICAL, PHYSICAL & ENGINEERING SCIENCES